*infrastructures*

*Article*

# First Level Pre- and Post-Earthquake Building Seismic Assessment Protocol Based on Dynamic Characteristics Extracted In Situ

**Spyros Damikoukas [1,2,†], Stavros Chatzieleftheriou [2,†] and Nikos D. Lagaros [1,*,†]**

1 Institute of Structural Analysis and Antiseismic Research, School of Civil Engineering, National Technical University of Athens, 9, Heroon Polytechniou Str., Zografou Campus, GR-15780 Athens, Greece
2 Unquake P.C., 6, Michali Karaoli, GR-17235 Dafni, Greece
* Correspondence: nlagaros@central.ntua.gr; Tel.: +30-210-772-2625
† These authors contributed equally to this work.

**Abstract:** The present work is concerned with the introduction of a new first level pre- and post-earthquake seismic assessment protocol for buildings that relies on the use of recorded structural response. As earthquakes represent a constant and unpredictable threat for the building stock around the globe, the protocols already in use for assessing the risk should be revised and should also take into account the information hidden in data recorded in the field. Nowadays, data collection does not require expensive equipment and over-qualified personnel. In this direction, the proposed seismic assessment protocol aims to illustrate the ease of widely adopting Structural Health Monitoring (SHM) equipment (e.g., accelerographs), based on the work that has been carried out over the past years on subjects related to earthquake risk estimation. Building taxonomy and damage estimation, like those found in Hazus®–MH and other hazard assessment tools, can be enriched and modified properly to distinguish and classify the very earthquake-prone buildings from the others, and tag them for further assessment and rehabilitation as seismic codes suggest.

**Keywords:** first level earthquake assessment protocols; structural health monitoring; building taxonomy; experimental dynamic characteristics; vulnerability; fragility; performance-based assessment



**Citation:** Damikoukas, S.; Chatzieleftheriou, S.; Lagaros, N.D. First Level Pre- and Post-Earthquake Building Seismic Assessment Protocol Based on Dynamic Characteristics Extracted In Situ. *Infrastructures* **2022**, *7*, 115. https://doi.org/10.3390/infrastructures7090115

Academic Editor: Denise-Penelope N. Kontoni

Received: 17 August 2022
Accepted: 26 August 2022
Published: 31 August 2022



## 1. Introduction

Earthquakes represent one of the most devastating natural hazards. Annually, they are responsible for the death of about 40,000 people; on average worldwide for the period 2000–2019, thousands of people were left homeless and the lives of millions more around the world were irreparably hit. Each year, in U.S. three people, on average for the period 1990–2019, lose their lives due to earthquakes. According to the U.S. Geological Survey (USGS), each year half a million earthquakes occur worldwide; nevertheless, not all countries have the same seismic risk [1,2]. Since 1990, 4500 seismic events of magnitude greater than 6.0 have been recorded, corresponding to around 152 events of magnitude 6.0 each year worldwide [3].

When earthquakes strike, there is no time for reaction; survival is related to specific factors. Governments issue guidelines for people like the Earthquake Safety Checklist [4] and launch campaigns like Ready Campaign [5], a National public service educational campaign since 2003. Despite the importance of people's awareness, the core anti-seismic measure against earthquakes is and should be designing earthquake-resistant structures. During the last decades, building codes have been improved and enriched with years of anti-seismic research and development concerning disaster faults. Admittedly, regulations used to design and construct the built environment have been playing an important role in the extent of the damages caused by earthquakes. Despite the progress, the need for continuous improvement of anti-seismic regulations remains. However, when it comes to comparing existing mega-scale building infrastructure of cities to future ones, there are some differences. Firstly, it is not economically feasible to rely on structural assessment reports common for all buildings and to the extent it is possible, there are obstacles, not only economical but architectural ones, in how many structural interventions can be made and how they will be integrated [6]. Therefore, structural assessment is divided into several levels. The first one refers to the evaluation of the seismic safety of a large inventory of buildings quickly and inexpensively, with minimum access to the buildings, and the determination of those buildings that require a more detailed examination. In this direction, many probabilistic risk/loss assessment methodologies have been introduced to prioritize risk mitigation actions, emergency planning, and management of related financial commitments [7,8]. However, in order to reduce the uncertainties, a clearer view of the inventory of assets (i.e., buildings) is required. With this purpose, a first taxonomy about the building stock was made. This first level assessment is adopted by FEMA P-154, denoted as Rapid Visual Screening (RVS) of Buildings for Potential Seismic Hazards [9]. Then, there are next levels, where critically acclaimed buildings are to be assessed in more detail and be retrofitted if needed. Retrofits should be in high priority for risky buildings, and structures in general, as they can potentially save huge amounts of money compared to rebuilding from the ground [10].

In earthquake-prone countries such as Greece, second and third levels of assessment protocols already exist for the pre-seismic inspection of public buildings (e.g., the guidelines of the Greek Earthquake Planning and Protection Organization [11]). The purpose of the second level seismic inspection in Greece is the re-hierarchical calibration of public buildings that, from the macroscopic first level seismic inspection [12], received a score below a prescribed limit. The second level inspection is an approximate but reliable process of assessing the seismic capacity and the seismic adequacy of existing buildings in relation to the seismic requirement, as defined by the modern code provisions. The outcome of this level of inspection is the so-called "Check Priority Index $\lambda$" of the building. This index denotes (in an approximate way) the degree of inadequacy for the specific building in terms of structural capacity and consequently the order of priority for the third level of assessment, i.e., the preparation of valuation studies and redesign (reinforcement) of a limited number of buildings according to the budget capacity of the relevant body.

Meanwhile, Structural Health Monitoring (SHM) has matured, and recent research has shown that now its results can begin to be widely adopted in engineering studies and analyses. Specifically, in the work by Standoli [13], it can be seen that a fine calibration of Finite Element (FE) models by data derived from non-destructive methodologies can be achieved, making analyses reliable in the absence of other destructive methodologies. Cases like buildings of cultural heritage, where human intervention can be as subtle as possible, show how nondestructive experimental methods are able to shine and establish often-uncertain parameters with a good grade of confidence concerning analytical methods. Two experimental methodologies are currently available: (i) the Experimental Modal Analysis (EMA), and (ii) the Operation Modal Analysis (OMA). In the first case, a known excitation is applied to the structure and its response is monitored; it is mostly used in laboratories [14] or structures types, such as bridges [15], where it is feasible. Speaking of feasibility, it should not be omitted that those input excitation machines should usually be considered as heavy, costly and with the possibility of generating local cracks in existing structures. On the other hand, the Operation Modal Analysis (OMA) consists of Ambient Vibration Testing (AVT), which involves construction vibration due to ambient sources. It grants the possibility to study in full scale buildings [16] while it is under its normal operation conditions, concerning load and operation aspects. As shown in works by Beskhyroun [17–19], a very good agreement was observed between the dynamic characteristics obtained using FE analysis and the experiments.

In this work, a new first level building seismic assessment protocol is introduced based on dynamic characteristics extracted in situ that is implemented through a novel methodology described subsequently in this study. The results of this methodology then are compared to the earthquake performance of calibrated building models. The remainder of this paper is organized as follows. Section 2 generally describes in detail all the steps for the use of the proposed screen and measures the first level pre- and post- seismic assessment methodology. Section 3 discusses the implementation of the proposed methodology in various buildings in Attica province in Greece along with the results obtained. A detailed numerical validation of the proposed methodology is provided in Section 4; it is carried out over two real-word building case studies. The paper concludes with some final remarks given in Section 5.

## 2. The Screen and Measure First Level Pre- and Post-Seismic Assessment (SMSA) Methodology

As was mentioned earlier, governments have issued guidelines for people for the case of an earthquake event, such as the Earthquake Safety Checklist [4], and have launched campaigns like Ready Campaign [5], a National public service educational campaign since 2003. In this direction, herein is proposed the screen and measure first level pre- and post-seismic assessment (SMSA) methodology; in this part of the study the novel screen and measure first level seismic assessment (SMSA) methodology is presented. The steps of the SMSA methodology are described below, and it is schematically presented in Figure 1:

1. *Site visit and installation of equipment*: (i) fast-track inspection of the building, (ii) building taxonomy based on several parameters, i.e., construction date, height, construction material, (iii) installation and operation of three-dimensional accelerograph on building top.
2. *Operational Modal Analysis*: (i) collection and automated treatment of measurements, (ii) derivation of building fundamental elastic frequency after statistical manipulation of ambient vibration data (e.g., averaging, cut-off strong excitations, etc.).
3. *Performance Analysis*: (i) correction of elastic dominant frequency to an effective sort based on pushover curves of taxonomy in order to take into account elastoplastic behavior, (ii) targeted displacement is computed from the relation proposed in FEMA 356 [20] as well as in the Greek Code of Interventions on RC buildings called "KAN.EPE" [21], (iii) calculation of probability of being in or exceeding a given damage state (i.e., slight, moderate, extensive, complete) based on estimated interstory drifts for a specific earthquake scenario.

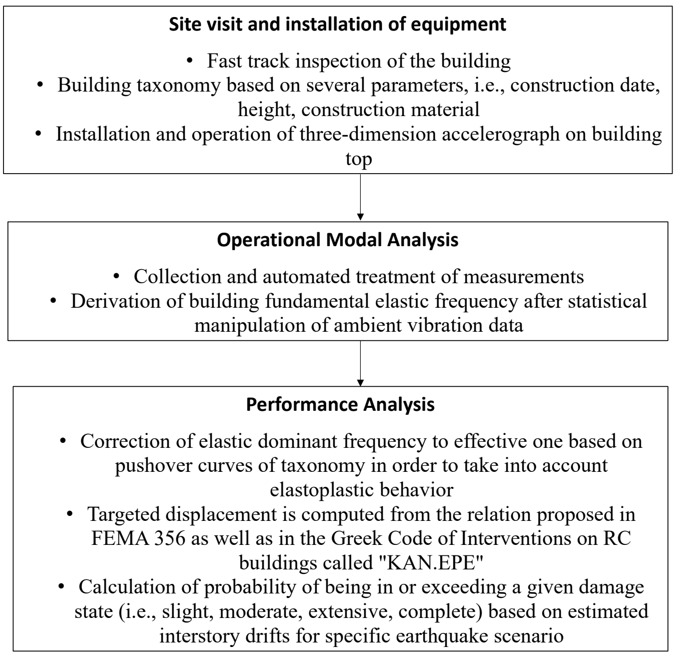


**Figure 1.** Flowchart of the SMSA methodology.

In this part of the study, it is worth mentioning the advantage of the SMSA methodology over the existing first level seismic assessment protocols, as it utilizes more experimental (in situ collected) data (see Operational Modal Analysis, Section 2.2) compared to the rapid visual-screening-based procedures. Therefore, the use of the recorded data in conjunction with information provided through an SDOF-based model procedure represents a more *objective* procedure rather than just a *subjective* one that relies more on the engineer's experience. Although the behavior estimated based on an SDOF system can deviate from the correct sort (e.g., in the case of non-symmetric systems), SDOF systems are widely used in structural engineering design for obtaining a quick estimation of the structural response and using appropriate corrections (nonlinear related ones) the real response can be derived (e.g., N2, ATC-40, coefficient method, etc.). Even newer methods have been developed in order to take into account higher mode effects both in plan and in elevation by combining the results of the basic pushover analysis and those of the standard elastic modal analysis (N2 extended). Therefore, in the case of the proposed methodology, by applying two or more sensors on the same diaphragm, the asymmetric character (rotational modes) [22] can easily be distinguished and therefore the results can be corrected if needed.

### *2.1. Site Visit and Installation of Equipment*

#### 2.1.1. Building Inspection

Firstly, a site visit is required for performing a fast inspection of the building under investigation. This inspection includes the determination of independent structural systems of the building, the existence of construction flaws and/or inadequate maintenance. Moreover, the building height is measured from the the ground level to the top story, along which the building is free to oscillate. If there is any visible damage, this is also noted.

#### 2.1.2. Building Classification

The classification of the building should be chosen in compliance with the building's fragility data that will be used later for performance analysis, and modified appropriately as will be shown subsequently. This modification refers to the correction of the typical response curve chosen, based on the measured elastic frequency of the building under consideration. In the context of the present study, a complete and reliable database of building stock and the expected seismic behavior is used; this is summarized in the Multi-hazard Loss Estimation Methodology Earthquake Model Hazus®–MH 2.1 Technical Manual [23]. The allocation of the buildings into classes is based on the following features:

- Material (e.g., masonry, steel, concrete),
- Structural system (e.g., moment frames, shear walls),
- Seismic design level (i.e., the level of seismic design code used, moderate-code, low-code or pre-code design levels),
- Height and number of stories (e.g., low-rise, mid-rise or high-rise).

There have been recent efforts at creating performance databases that compile post-earthquake assessments for different building taxonomies [24,25].

#### 2.1.3. Installation and Operation of the Accelerograph

After site visit and building classification, at least a two-channel accelerograph needs to be installed—it is suggested it be installed at the top level of the building—for recording its response when subjected to microtremors. The two channels are oriented in the main building directions of the X–Y plane, which are usually defined by the vertical structural elements such as columns and shear walls. The building's response excited by ground ambient noise is usually in the range of tens to hundreds of μgs. In the current study the Unquake® accelerograph [26] is used; this is a three-dimensional accelerograph with an operating acceleration range $\pm 2$ g (Figure 2). The logging is continuous and local in all three axes; with a resolution of 3.81 μg and a sampling rate of 250 Hz. The Unquake® accelerograph is equipped with a microSD card form factor with a storage size up to 128 Gb. The high resolution is useful when recording the ambient vibration-based responses of a building, especially in cases of low-rise ones (up to 2–3 storeys). The ambient response in acceleration terms at the top level of low-rise buildings is in the order of tens to hundreds of $\mu g_s$. An important issue that also needs to be taken into account is the noise levels of the sensor; the higher the noise level, the higher the time needed for averaging the signal windows in order to obtain the mean value of the FFT frequency spectrum. In the cases examined in this study, the levels of noise for the sensor used were of 22.5 $\mu g_s/\sqrt{\text{Hz}}$. Moreover, the sampling rate with respect to the Whittaker–Nyquist–Shannon sampling theorem [27] must be at least double the demanding frequency spectra to be measured. So in the case of buildings where the frequencies of interest (not only the first ones) vary up to 50–60 Hz, a sampling rate higher or equal to 125 Hz should be adequate.

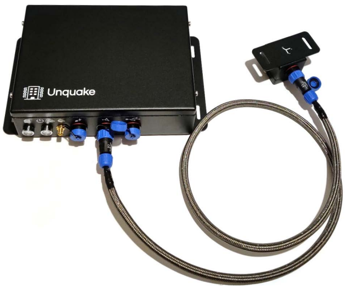


**Figure 2.** Unquake accelerograph.

With respect to the installation of the accelerograph, the accelerometer should be placed at the top level, i.e., the last slab of significant dimensions (see Figure 3). Where this is not feasible, the accelerograph can be installed vertically on the side of a load-bearing element (e.g., column, beam). It is preferred to install the accelerometer directly on the reinforced concrete element after the plaster coat has been removed. Alternatively, if the surface is judged intact (without cracking through), it can also be installed on the top layer, including paint. The installation is implemented by providing a strong adhesive that stabilizes a metal plate within a few minutes. The sensor (accelerometer) is then mounted on the particular plate with a powerful magnet and is suitably oriented. However, an alternative and easier way is the use of BluTack (Bostik, Leicester, UK) [28].

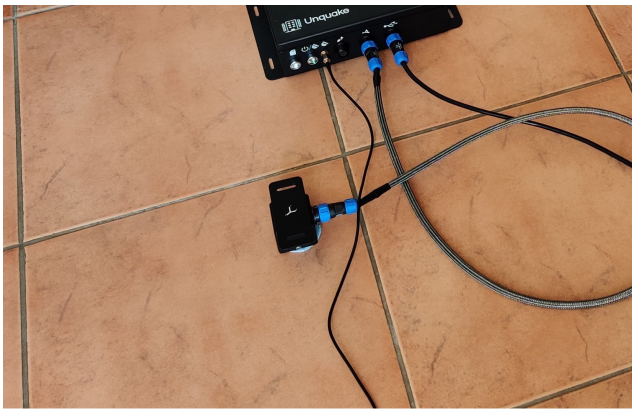


**Figure 3.** Unquake accelerometer placement with BluTack.

An approach aiming to integrate the soil–structure interaction (SSI) issue into the proposed methodology is to use multiple sensors vertically allocated throughout the building structure, especially one at the basement and one at the top of the structure in order to decouple the soil effects from the remaining structure [29,30]. Given that the earthquake demand (i.e., the spectral acceleration) is computed from the combined system's eigenperiod, the proposed methodology should be corrected in that perspective. As part of the proposed methodology, only in cases where the SSI contribution is significant is it suggested that the capacity curve developed be corrected as follows: in such cases, sensors should also be installed at the ground level and the rocking component contribution on the structural response should be removed from the target displacement.

### *2.2. Operational Modal Analysis*

After some hours, the building is visited again to uninstall the accelerographs and collect the data. Afterwards, the steps of the proposed methodology for deriving the frequency components of the recorded signals are:

1. The standard deviation for each measurement file is calculated.
2. A window of 30 s is selected.
3. The standard deviation for the current window is calculated. If this is less than the standard deviation of the corresponding file, Fast Fourier Transform (FFT) is performed. Otherwise, the window moves without overlapping with the previous one. This step is necessary in order to distinguish ambient noise measurements from all those not subject to the assumption of white noise, such as stronger local (and not) excitations.
4. For the accepted windows of previous steps, FFTs are calculated, the amplitude of each of these windows is summed and the mean value of those is calculated.
5. From the peaks of the averaged Fourier spectra, the dominant eigenfrequencies (natural periods) of the structure (lower values) in each direction are determined. There are also some peaks at higher frequencies that are related to local eigenmodes of the structure. Observing the eigenfrequencies, they are unchanged over the period of the file measurements under consideration.

### *2.3. Performance Analysis*

The proposed methodology is based on the philosophy of the modern seismic assessment regulations (e.g., Eurocode 8, FEMA, etc.). In these regulations, the building's response is simulated by the response of an equivalent single degree of freedom oscillator that is excited by an earthquake. In cases of small excitation, the response of the oscillator will be consistent with the measured frequency and a characteristic damping coefficient according to the type of construction. In cases of larger excitations, due to the non-linear response of the structure (e.g., crack openings in concrete, hysterical damping, etc.) and depending on the building type, the basic natural frequency and damping coefficient are corrected according to the code guidelines. Target displacements can be estimated by means of approximate methods like ATC-40 [31], N2 [32], N2-extended [33] and the coefficient method [20], or using modal non-linear static analyses also known as modal pushover method. In accordance with the proposed methodology, a combination of the coefficient method and pushover curve results of typical buildings are used.

#### 2.3.1. Correction of Elastic Dominant Frequency

Given the building classification defined in the previous step, a pushover curve (in Acceleration-Displacement Response Spectrum (ADRS) form) is approximated based on the Yield Capacity Point and Ultimate Capacity Point of the properly chosen typical building type of Hazus®–MH 2.1 Technical Manual and through an appropriately *fitted polyline curve*. Subsequently, the curve is corrected through the following procedure: each branch of this polyline has a reduced slope proportional to the initial branch denoting the linear behaviour. The condition required for the first part of the polyline fit is that its slope at zero Spectral Displacement should be equal to the measured fundamental elastic eigenfrequency. The rest of the branches are corrected correspondingly, so that the ratio of the branches' slopes before and after correction remains unchanged. After fitting the pushover curve, bi-linearization of the corrected curve is implemented and a different (to the typical one) effective period is derived, which will be used for the calculation of the target displacement. In this way, a modified typical capacity curve is used based on in situ same-type building measurements. The reason for correcting the pushover given by Hazus®–MH 2.1 is that the ambient vibration measurements required by the proposed methodology refer to buildings' responses at a complete elastic state, at which the load bearing building frame is mainly subjected to static vertical loads. Due to a lack of horizontal seismic forces during monitoring, the vertical structural elements are subjected mostly to compression and thus stiffness is at its highest possible degree; therefore, materials operate mostly elastically.

### 2.3.2. Target Displacement Calculation

Given that the effective period for the building of interest is known, the coefficient method can be used for any seismic scenario (demand) in order to calculate target displacement (capacity). The coefficient method is described in FEMA 356 [20] and the target displacement is calculated with the following expression Equation (1):

$$\delta t = C_0 C_1 C_2 C_3 S_\alpha \frac{T_e^2}{4\pi^2} g\ , \tag{1}$$

where $C_0$ is the modification factor to relate spectral displacement of an equivalent SDOF system to the roof displacement of the building MDOF system, $C_1$ is the modification factor to relate expected maximum inelastic displacements to displacements, $C_2$ is the modification factor to represent the effect of the pinched hysteretic shape, stiffness degradation and strength deterioration on maximum displacement response, $C_3$ is the modification factor to represent increased displacements due to dynamic P-Δ effects, $S_\alpha$ is the response spectrum acceleration at the effective fundamental period and damping ratio of the building in the direction under consideration, $T_e$ is the effective fundamental period of the building in the direction under consideration. In the method proposed, $C_0$ is omitted, as the comparison to the performance levels is made in spectral terms.

The performance levels of Hazus®–MH that are adopted by the proposed methodology are represented by four damage states—slight, moderate, extensive and complete—which are defined separately for structural and nonstructural systems of the building. For each material, structural type, building height and level of seismic code, damage states are described accordingly. For each one of these, a median value of the Potential Earth Science Hazards (PESH) demand parameter is provided (i.e., either spectral displacement, spectral acceleration, PGA or PGD) that corresponds to the threshold of the damage state and according to the variability associated with that damage state. In that way, the conditional probability of a particular damage state, *ds*, being exceeded or not, given the calculated spectral displacement, $S_d$ (or other PESH parameter), is defined with the following expression Equation (2):

$$P[ds|S_d] = \Phi\left[\frac{1}{\beta_{ds}} ln(\frac{S_d}{\overline{S}_{d,s}})\right]\ , \tag{2}$$

where $\overline{S}_{d,s}$ is the median value of spectral displacement at which the building reaches the threshold of damage state, *ds*, $\beta_{ds}$ is the standard deviation of the natural logarithm of spectral displacement for damage state, *ds*, and $\Phi$ is the standard normal cumulative distribution function. Median spectral displacement (or acceleration) values and the total variability are developed for each of the model building types and damage states of interest by the combination of performance data (from tests of building elements), earthquake experience data, expert opinion and judgment as proposed by Hazus®–MH. Specifically, the values of the parameters can be found in the corresponding Tables of the Hazus®–MH Technical Manual (i.e., Table 5.9a–d of [23]).

## 3. Experimental Cases for 27 RC Buildings

In order to verify the efficiency of the SMSA methodology, it was applied to 27 reinforced concrete (RC) buildings located in Attica province of Greece (see details of this investigation in Table 1 and Figure 4). In Table 1, *SS* stands for structural system, $Freq_r$ and $Freq_m$ denote the recorded (measured) elastic and modified (SDOF) frequency, respectively, and $Freq_{EC8}$ is the frequency derived through the expression of EC8. After visiting each site and proceeding with accelerograph placement, the fundamental frequency of each building, elastic and uncorrected, was measured. With the use of the proposed methodology, the modified elastic frequency (Hz) is calculated. At this point, it is worth mentioning that various empirical relationships are given by earthquake design codes in Europe (EC8-1 [34]) and North America (UBC97 [35] and NBCC-2005 [36]) that can be used for performing quick pre-design calculations and estimations. For completeness, the measured elastic fundamental frequencies are presented below for 27 buildings in Attica province of Greece. Within this context, the frequency for each of these buildings is also calculated based on the Eurocode 8 expression of Equation (3) below:

$$T_1 = C_t \times H^{\frac{3}{4}} \tag{3}$$

where $C_t$ is taken as equal to 0.085 for moment resistant space steel frames, 0.075 for moment resistant space concrete frames and for eccentrically braced steel frames, and 0.050 for all other types of structure. In order to examine the accuracy of the empirical expressions of the design codes used for calculating the first period of a building, the investigation performed is provided in Appendix A, where the parameters of the above equation used by standards are examined in correlation with the experimental data of the 27 RC buildings through sensitivity analysis of $C_t$ and $\beta$.

**Table 1.** Experimental data collected from 27 RC Buildings.

| No. | *SS* | Design Year | Height (m) | $Freq_r$ (Hz) | $Freq_m$ (Hz) | $Freq_{EC8}$ (Hz) | Pds1 | Pds2 | Pds3 | Pds4 | Pds5 |
|---|---|---|---|---|---|---|---|---|---|---|---|
| 1 | C3 | 1992 | 21.00 | 3.90 | 3.49 | 1.36 | 0.78 | 0.17 | 0.05 | 0.00 | 0.00 |
| 2 | C3 | 1991 | 17.80 | 3.90 | 3.37 | 1.54 | 0.56 | 0.28 | 0.14 | 0.01 | 0.00 |
| 3 | C3 | 1987 | 18.00 | 3.30 | 2.82 | 1.53 | 0.47 | 0.31 | 0.19 | 0.02 | 0.01 |
| 4 | C1 | 1970 | 28.00 | 2.00 | 1.62 | 1.10 | 0.55 | 0.21 | 0.19 | 0.04 | 0.01 |
| 5 | C1 | 1970 | 25.50 | 1.10 | 0.88 | 1.17 | 0.16 | 0.22 | 0.40 | 0.17 | 0.05 |
| 6 | C3 | 1987 | 7.50 | 6.23 | 4.80 | 2.94 | 0.62 | 0.22 | 0.13 | 0.03 | 0.00 |
| 7 | C3 | 1970 | 10.90 | 6.03 | 4.85 | 2.22 | 0.71 | 0.19 | 0.09 | 0.01 | 0.00 |
| 8 | C3 | 1981 | 10.70 | 5.83 | 4.68 | 2.25 | 0.68 | 0.21 | 0.10 | 0.01 | 0.00 |
| 9 | C3 | 1974 | 7.40 | 6.63 | 5.10 | 2.97 | 0.66 | 0.20 | 0.12 | 0.02 | 0.01 |
| 10 | C3 | 1967 | 13.00 | 3.87 | 3.17 | 1.95 | 0.45 | 0.29 | 0.22 | 0.03 | 0.01 |
| 11 | C3 | 1969 | 9.00 | 4.10 | 3.23 | 2.57 | 0.24 | 0.25 | 0.33 | 0.15 | 0.03 |
| 12 | C3 | 1965 | 20.70 | 2.77 | 2.47 | 1.37 | 0.43 | 0.32 | 0.21 | 0.03 | 0.01 |
| 13 | C3 | 1964 | 7.20 | 7.13 | 5.47 | 3.03 | 0.55 | 0.24 | 0.17 | 0.04 | 0.00 |
| 14 | C3 | 1971 | 13.40 | 5.60 | 4.60 | 1.90 | 0.57 | 0.26 | 0.15 | 0.02 | 0.00 |
| 15 | C3 | 1976 | 13.00 | 4.90 | 4.01 | 1.95 | 0.62 | 0.24 | 0.12 | 0.01 | 0.00 |
| 16 | C3 | 1968 | 9.60 | 4.53 | 3.59 | 2.44 | 0.46 | 0.27 | 0.21 | 0.05 | 0.01 |
| 17 | C3 | 1982 | 7.00 | 8.37 | 6.40 | 3.10 | 0.78 | 0.15 | 0.06 | 0.01 | 0.00 |
| 18 | C3 | 1984 | 17.60 | 3.34 | 2.88 | 1.55 | 0.47 | 0.31 | 0.19 | 0.02 | 0.01 |
| 19 | C3 | 1960 | 11.00 | 3.67 | 2.95 | 2.21 | 0.23 | 0.26 | 0.34 | 0.13 | 0.03 |
| 20 | - | 1972 | 12.00 | 4.63 | - | 2.07 | - | - | - | - | - |
| 21 | - | 1974 | 11.00 | 5.53 | - | 2.21 | - | - | - | - | - |
| 22 | - | 1959 | 12.00 | 5.43 | - | 2.07 | - | - | - | - | - |
| 23 | - | 1959 | 15.50 | 3.40 | - | 1.71 | - | - | - | - | - |
| 24 | - | 1984 | 11.10 | 6.90 | - | 2.19 | - | - | - | - | - |
| 25 | - | 1981 | 12.60 | 4.17 | - | 1.99 | - | - | - | - | - |
| 26 | - | 1976 | 13.00 | 2.50 | - | 1.95 | - | - | - | - | - |
| 27 | - | 1980 | 7.20 | 4.61 | - | 3.03 | - | - | - | - | - |

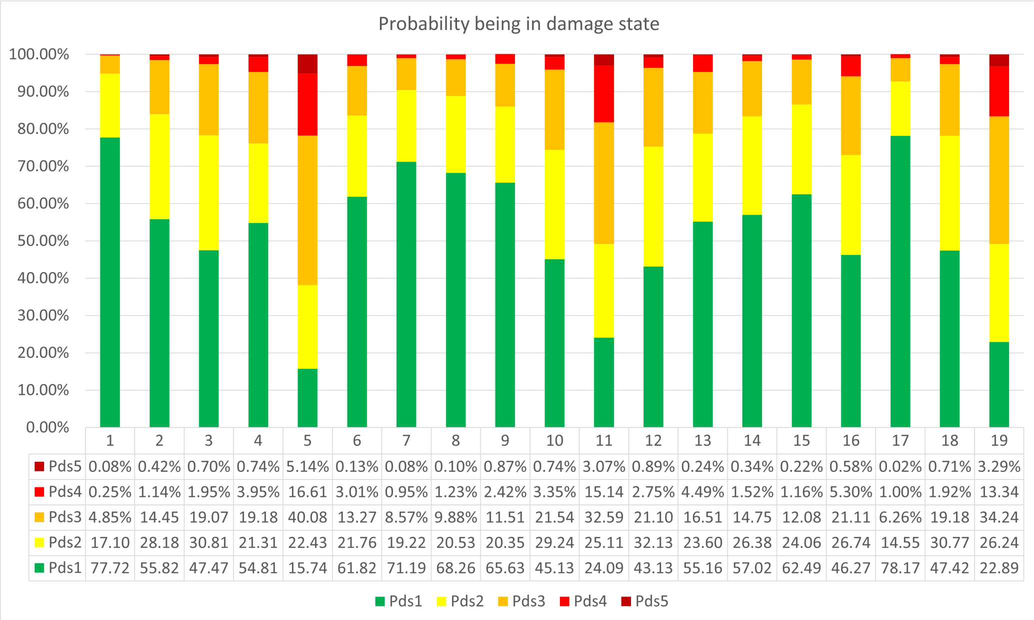


**Figure 4.** Probability of damage state for each of 19 RC buildings.

The building taxonomy for the appropriate structural system ($SS$) was based on Hazus®–MH 2.1 (see description in paragraph 5.2.1 of the Technical Manual [23]). Most buildings were chosen as C3 category due to the existence of unreinforced masonry infill walls. This reinforced concrete building with infill walls is also the most common type of general building stock in cities of Greece. Two cases of C1 category, which means reinforced concrete moment resisting frames according to Hazus®–MH, were two relatively tall buildings with many modifications to their floor clearances as traditional infill walls had been replaced with dry walls and other modular office walls which do not contribute in the same way to the whole building's stiffness. The base shear used for most of the 27 buildings was obtained from the response spectrum for soil type B (stiff soil $\theta = 1.0$, with characteristic periods $T_1 = 0.15$ s and $T_2 = 0.60$ s); there were deposits of very dense sand, gravel or very stiff clay for several tens of meters in thickness as assumed. Moreover, the importance factor $\gamma_I$ was taken equal to 1.0, while the damping correction factor is equal to 1.0 since a damping ratio of 5% was considered.

Moreover, it was expected that the difference between the uncorrected frequency ($Freq_r$) and the one proposed with the EC8 empirical relationship ($Freq_{EC8}$) would be very different. The main reason is that EC8.1 for each analysis procedure takes into account the degradation concerning the stiffness of structural members during the design seismic event. Based on EC8-1, the geometrical cross section is reduced to 50%, so frequency quantities are reduced accordingly. Even after our correction of the measured frequencies to $Freq_m$ as referred to in Table 1, it can be noticed that a difference compared to EC8 empirical ones still exists. However, as can be seen in Table A1, our measurements show a close match to ones predicted by Chiauzzi et al. [37]. For investigating how different empirical eigenperiods are, sensitivity analysis of Equation (3) used in EC8-1 (Table A2) and KAN.EPE (Table A3) was conducted in correspondence with the experimental data.

## 4. Numerical Validation with FEM (the 2 Building Case Studies)

In order to present the efficiency and applicability of the proposed first level building seismic assessment methodology, two buildings are studied. Both of them are real-world test cases and they are located in Attica province of Greece; therefore, they were designed based on the Greek seismic design codes. In this section, details about the two structures and any assumptions made will be presented together with the results obtained through the implementation of the assessment methodology.

*4.1. Building 1*

The first building, shown in Figure 5, refers to a reinforced concrete (RC) building based on a moment frame structural system with infill walls. It was designed and constructed in two phases; during the first one, the first three floors were constructed around 1984, while they were designed using the seismic design code of 1959 that is the first seismic design code of Greece. In its final form constructed around 1995, it consists of a basement, ground floor, mezzanine and five more floors. Its height from the ground level to the top one is 20.80 m. The finite element (FE) model and the analyses required were carried using SCADA Pro 2018 structural analysis and design software. A typical reinforcement detailing of beams located at the upper floors for Building 1 can be found in Figure 6.

**Figure 5.** Building 1 street view.

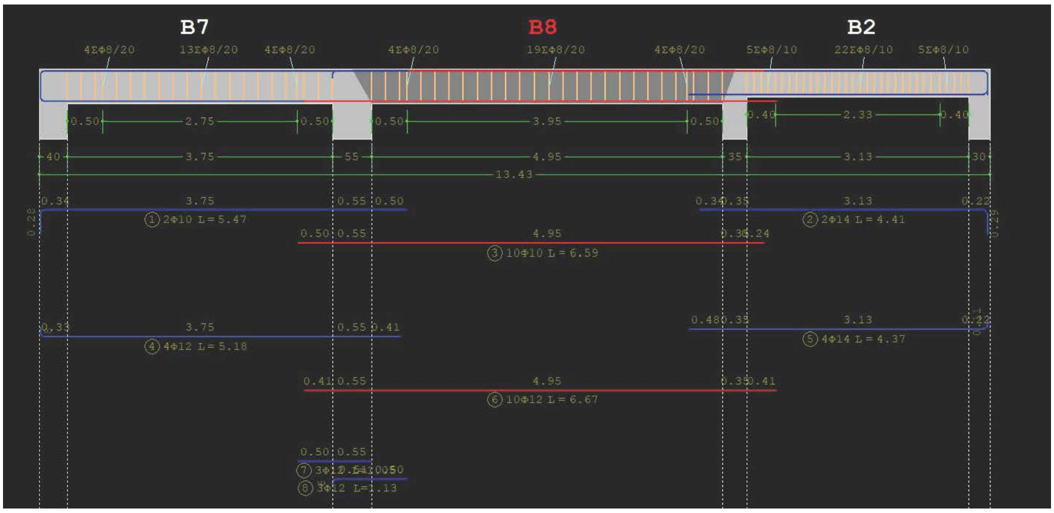


**Figure 6.** A typical detailing of reinforcement on the upper floor of Building 1.

After the on-site visits, properties and loads of the structures were estimated (see Table 2). During these visits, accelerographs were installed on the top level of Building 1 and the dominant frequencies per direction were extracted; in Figure 7, the average FFT magnitudes for each direction of Building 1 are shown. The next step was to calibrate the model in order to match the measured eigenfrequencies. The parameters to be calibrated were the imposed loads along with the modulus of elasticity for concrete and infill walls. Given that the imposed loads were parameters to be calibrated in order to approximate the real loads during the measurements, the value used for the imposed loads was equal to 1 kN/m$^2$. The infill walls were also introduced in the model and their modulus of elasticity was a parameter. As the structure proved to be more stiff than the initial model, the moments of inertia of the cross sections were assumed to be equal to that of a non-cracked section (i.e., 100%) in order to simulate ambient vibration conditions (microtremors), and the moduli of elasticity for concrete and walls had to be raised up to 40% of their original values. Afterwards, during the assessment phase of the building, the load values and the moment of inertia percentage were restored to the values proposed in Eurocodes 1 and 2. The seismic assessment for the full-scale model was performed by means of nonlinear pushover analysis. The plastic hinge rotation moment equations used along with the member shear strength calculations were those described in the Greek Code of Interventions on RC buildings (KAN.EPE) [21].

**Table 2.** Details for building case studies 1 and 2.

| | Type | Building No. 1 | Building No. 2 |
|---|---|---|---|
| Material Properties | Concrete | $f_{ck}$ = 8 MPa | $f_{cm,cyl}$ = 31.0 MPa |
| | Steel Reinforcement | S400 | S400 |
| Seismic | Ductility Class | DCL | DC |
| | Ground acceleration $a_g$ (g) | 0.19 | 0.12 |
| | Importance factor $\gamma_i$ | 1 (Σ2) | 1 (Σ2) |
| Ground details | Category | B | B |
| | Foundation factor | 1.00 | 1.00 |
| | $\sigma_z$ (kN/m$^2$) | 200 | 200 |
| | $K_s$ (kPa/cm) | 300 | 300 |

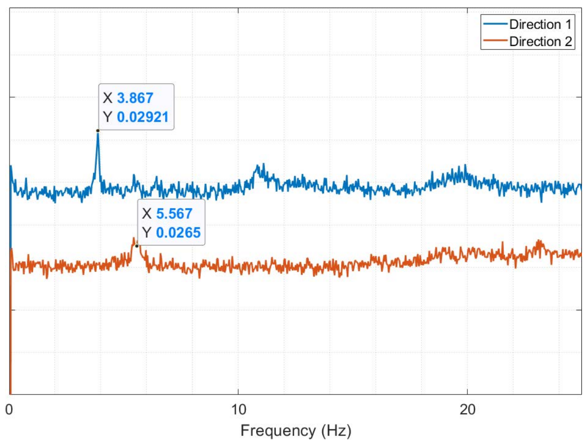


**Figure 7.** Average FFT magnitude for each direction in Building 1.

In order to compare the results obtained using the proposed methodology, two pushover analyses were performed along the two main directions. These analyses showed the building behaviour and damage level under specific earthquake scenarios; damage level is defined based on the percentage of damaged structural elements such as columns and beams. As the proposed methodology characterizes damage levels along the approximate pushover curves and in order to compare between them, similar damage levels should be appointed to the pushover curves. In order to do so the percentage of columns in performance level A (slight damages), B (extensive damages) or C (collapse) are depicted on the analytical pushover curves. Finally, the seismic demand is computed according to KAN.EPE and Equation (1) for both cases. The results of the methodology are depicted in Figure 8, and the seismic assessment of the full-scale model in Figure 9. The target displacement along with the final seismic assessment show satisfactory convergence between the proposed methodology and the code provisions. Comparing the estimated capacity curve (Figure 8) with the one developed through detailed models (Figure 9), it can be said that they match acceptably.

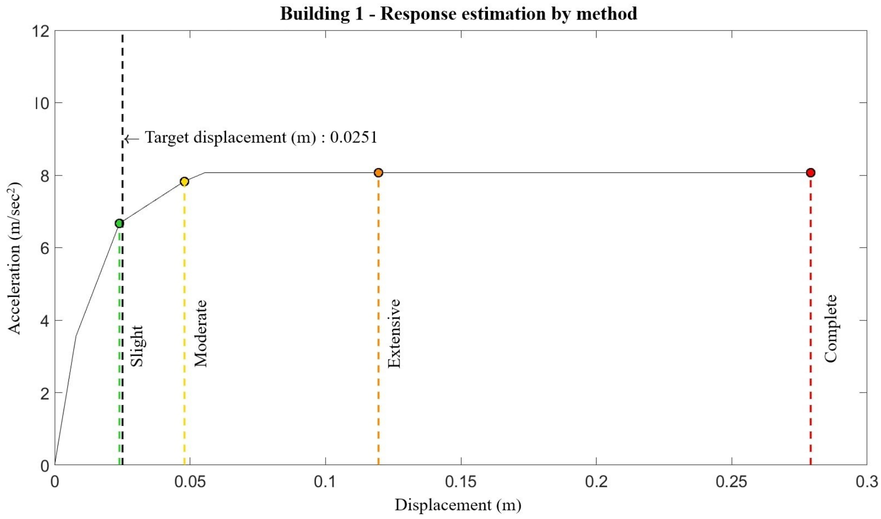


**Figure 8.** Building 1: Response estimation by means of the SMSA methodology.

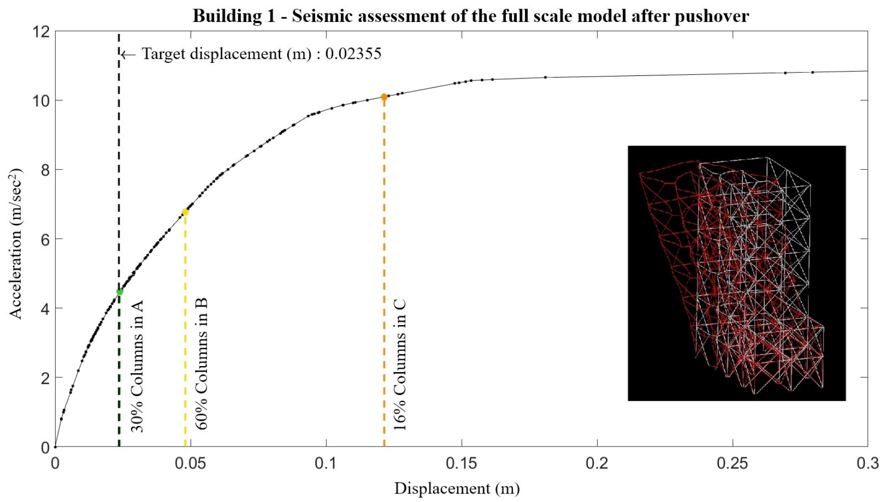


**Figure 9.** Building 1: Seismic assessment results of the full-scale model after pushover.

### *4.2. Building 2*

A similar comparative study was performed for Building 2, and is shown in Figure 10. Building 2 is also an RC structure with a moment frame structural system with infill walls. It was also designed using the seismic code of 1959, while it was constructed around 1975. It consists of a basement, ground floor and two floors, while its height is 10.65 m measured from the ground level. In accordance with Building 1, the FE model and the analyses required were carried out using SCADA Pro 2018 structural analysis and design software. During the on-site visits, accelerographs were also installed on the building and the dominant frequencies per direction were also extracted (see Figure 11). Furthermore, electromagnetic scanning of the reinforcement was implemented along with compression tests on specimens of concrete (Figure 12) extracted from the structure.

**Figure 10.** Building 2 street view.

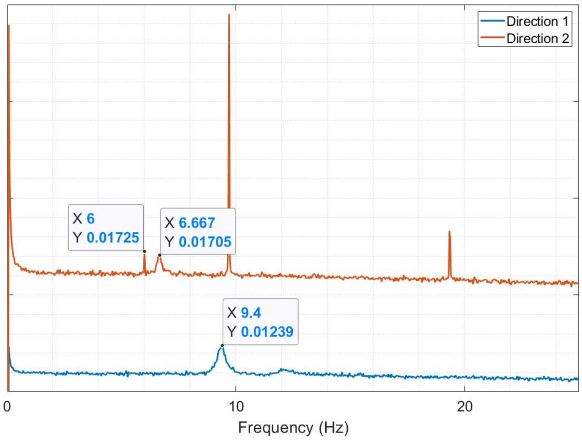


**Figure 11.** Building 2: Average FFT magnitude for each direction.

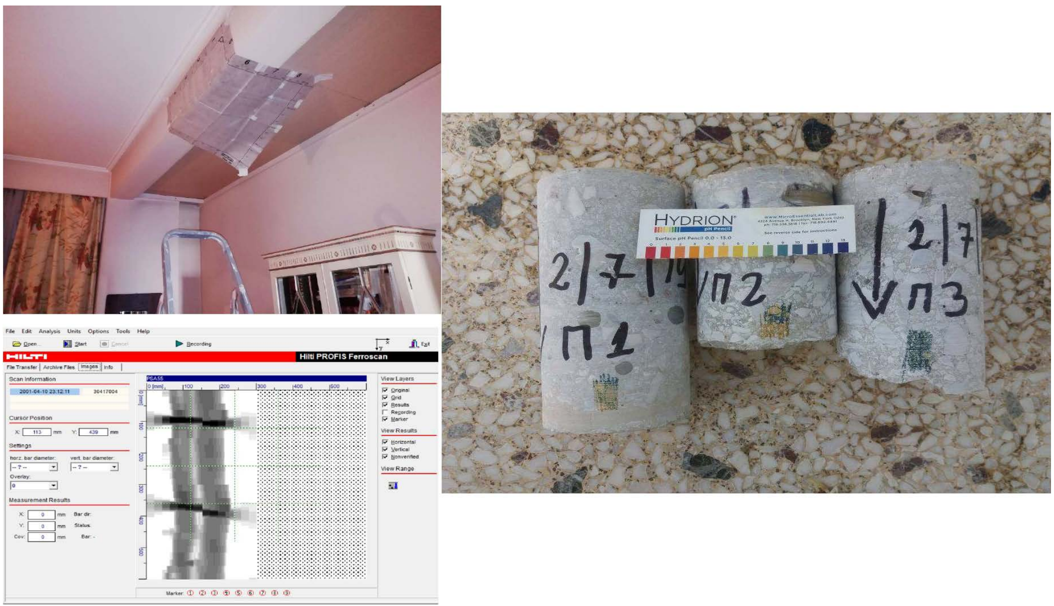


**Figure 12.** Building 2: Electromagnetic scanning of steel rebar in a beam and concrete specimens.

The values of the compression strength extracted for concrete for cylinder and cube are seen in Table 2. Reinforcement details from a typical column are shown in Figure 12. The full-scale model was calibrated based on a procedure similar to that implemented for Building 1 and the eigenfrequencies were matched to the measured ones. Subsequently, the values for loads and moments of inertia were restored to the values proposed by the

Eurocodes 1 and 2 and two pushover analyses of the full-scale model were performed. The results of the comparison of the full-scale model for Building 2 along with the ones computed by the proposed methodology are depicted in Figures 13 and 14. Similar to Building 1, the results obtained for Building 2 show satisfactory convergence both in terns of seismic demand as well as seismic assessment regarding all performance levels adopted. In addition, comparing the estimated capacity curve (Figure 13) with the one developed through detailed models (Figure 14), it can be said that they match acceptably.

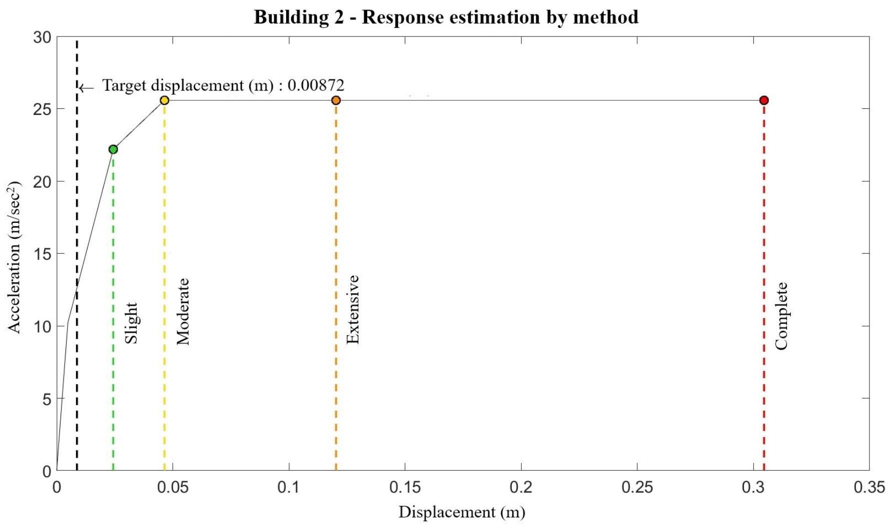


**Figure 13.** Building 2: Response estimation by method.

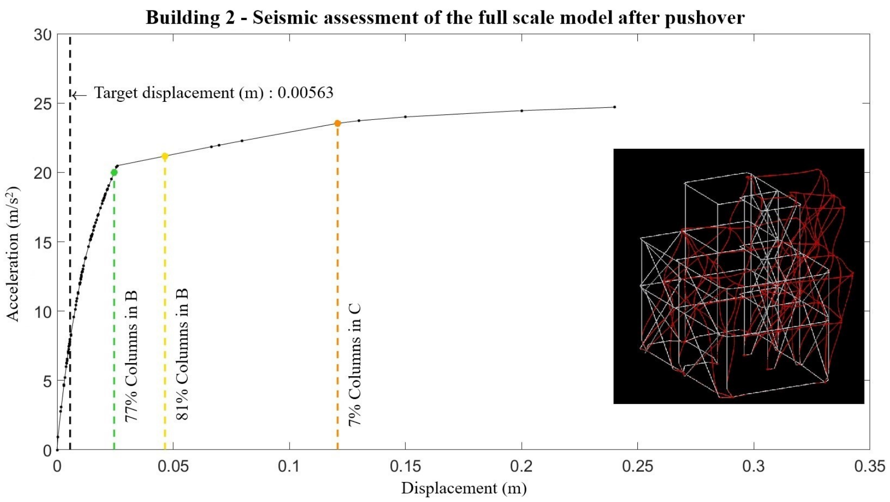


**Figure 14.** Building 2: Seismic assessment results of the full-scale model after pushover.

## 5. Conclusions

In this work, a new methodology is proposed for performing first level building seismic assessment that relies on the dynamic characteristics of the building extracted from in situ measurements. For depicting the capabilities of the proposed methodology, two real-world problems are employed where it was successfully applied. As shown, the proposed methodology estimates the probability of exceedance of a damage state for a building pretty successfully, as other traditional approaches require implementing analytical CAE models and pushover analyses. The building's frequency extraction is the core function of the proposed methodology; it differs from other pre- and post-earthquake fast-track building seismic assessment approaches, which mainly rely on plain taxonomy or visual inspection. It is worth underlining that the proposed methodology is not introduced as an assessment methodology that will replace CAE analyses and analytical methods, which however is a step further than the approaches needed and used for the quantification of seismic risk throughout building stock. Nowadays, the ease of using accelerographs widely in the field, processing efficiently and quickly the data on the go and in the end using real dynamic characteristics derived from buildings pave the way to adoption of innovative protocols in seismogenic countries around the world. Last but not least, an investigation of the empirical relationships used by codes for predicting effective fundamental periods showed that further calibrations to the parameters used can be made for matching building stock of various countries such as Greece, exploiting local differences in construction materials, practices and regulations.

## 6. Patents

Stavros Chatzieleftheriou, Spyros Damikoukas, Nikos D. Lagaros, US20220082717A1—Accelerograph and Embedded Protocol for Structural Health Monitoring of Civil Engineering Structures Regarding Earthquake Performance, US patent, 17 March 2022.

**Author Contributions:** Conceptualization, S.D., S.C. and N.D.L.; methodology, S.D. and S.C.; software, S.D.; validation, S.D. and S.C.; investigation, S.D. and S.C.; resources, N.D.L.; data curation, S.D. and S.C.; writing—original draft preparation, S.D.; writing—review and editing, S.D., S.C. and N.D.L.; visualization, S.D.; supervision, N.D.L.; project administration, S.C. and N.D.L.; funding acquisition, N.D.L. All authors have read and agreed to the published version of the manuscript.

**Funding:** This research has been financed by the ADDOPTML project: "ADDitively Manufactured OPTimized Structures by means of Machine Learning" (No: 101007595).

**Institutional Review Board Statement:** Not applicable.

**Informed Consent Statement:** Not applicable.

**Data Availability Statement:** Not applicable.

**Acknowledgments:** This research has been supported by the ADDOPTML project: "ADDitively Manufactured OPTi-mized Structures by means of Machine Learning" (No: 101007595) belonging to the Marie Skłodowska-Curie Actions (MSCA) Research and Innovation Staff Exchange (RISE) H2020-MSCA-RISE-2020. Their support is highly acknowledged.

**Conflicts of Interest:** The authors declare no conflict of interest.

## Abbreviations

The following abbreviations are used in this manuscript:

| | |
|---|---|
| ADRS | Acceleration-Displacement Response Spectrum |
| AVT | Ambient Vibration Testing |
| EMA | Experimental Modal Analysis |
| FEM | Finite Element Method |
| FEMA | Federal Emergency Management Agency |
| FFT | Fast Fourier transform |
| MDOF | Multiple Degree of Freedoms |
| OMA | Operation Modal Analysis |
| RC | Reinforced Concrete |
| RVS | Rapid Visual Screening |
| SDOF | Single Degree of Freedom |
| SHM | Structural Health Monitoring |
| SMSA | Screen and Measure first level Seismic Assessment methodology |
| USGS | U.S. Geological Survey |

## Appendix A. Experimental vs. Empirically Calculated 1st Eigenperiod

### *Appendix A.1. Trend Lines*

In the investigation presented in the following three Tables, a measure of the correctness is defined comparing the ratio of the eigenperiod derived through recordings over the corresponding estimation obtained by means of empirical expressions of the design codes. Specifically, in Table A1, $T_{amb}$ denotes the 1st eigenperiod derived based on structural response recordings due to ambient vibration, while $T_{EC8}$, $T_{KNP}$ refer to the values of the effective 1st eigenperiod derived through the expressions of EC8-1 (see Equation (3), that relies on the effective stiffness) and that of KAN.EPE (see the corresponding Equation (A2) provided in the following sub-section) design codes, while $T_{3033}$ refers to the fundamental elastic eigenperiod derived from the expression of (A1) through regression of experimental results for RC buildings in Canada, performed in the work by Chiauzzi et al. [37] and was presented in the WCEE2012 conference, respectively. Part of the information provided in Table A1 is also summarized in Figure A1 along with the trend lines for every case.

Below the expression from Chiauzzi et al. work [37] is also provided:

$$T_1(= T_{3033}) = 0.037 \times H^{0.76} \tag{A1}$$

where, the height $H$ is provided in meters ($m$) and $T_1$ is the fundamental elastic period for the Canadian RC buildings.

**Table A1.** Experimental and theoretical values of the effective 1st period for the 27 RC buildings.

| No. | $T_{amb}$ (s) | $T_{EC8}$ (s) | $T_{KNP}$ (s) | $T_{3033}$ (s) |
|---|---|---|---|---|
| 1 | 0.256 | 0.736 | 0.805 | 0.374 |
| 2 | 0.256 | 0.650 | 0.694 | 0.330 |
| 3 | 0.303 | 0.655 | 0.701 | 0.333 |
| 4 | 0.500 | 0.913 | 1.043 | 0.466 |
| 5 | 0.909 | 0.851 | 0.959 | 0.434 |
| 6 | 0.161 | 0.340 | 0.319 | 0.171 |
| 7 | 0.166 | 0.450 | 0.446 | 0.227 |
| 8 | 0.172 | 0.444 | 0.439 | 0.224 |
| 9 | 0.151 | 0.336 | 0.315 | 0.169 |
| 10 | 0.258 | 0.513 | 0.523 | 0.260 |
| 11 | 0.244 | 0.390 | 0.376 | 0.197 |
| 12 | 0.361 | 0.728 | 0.795 | 0.370 |
| 13 | 0.140 | 0.330 | 0.307 | 0.166 |
| 14 | 0.179 | 0.525 | 0.538 | 0.266 |
| 15 | 0.204 | 0.513 | 0.523 | 0.260 |
| 16 | 0.221 | 0.409 | 0.398 | 0.206 |
| 17 | 0.119 | 0.323 | 0.300 | 0.162 |
| 18 | 0.299 | 0.644 | 0.687 | 0.327 |
| 19 | 0.272 | 0.453 | 0.450 | 0.229 |
| 20 | 0.216 | 0.484 | 0.487 | 0.245 |
| 21 | 0.181 | 0.453 | 0.450 | 0.229 |
| 22 | 0.184 | 0.484 | 0.487 | 0.245 |
| 23 | 0.294 | 0.586 | 0.613 | 0.297 |
| 24 | 0.145 | 0.456 | 0.454 | 0.230 |
| 25 | 0.240 | 0.502 | 0.509 | 0.254 |
| 26 | 0.400 | 0.513 | 0.523 | 0.260 |
| 27 | 0.217 | 0.330 | 0.307 | 0.166 |

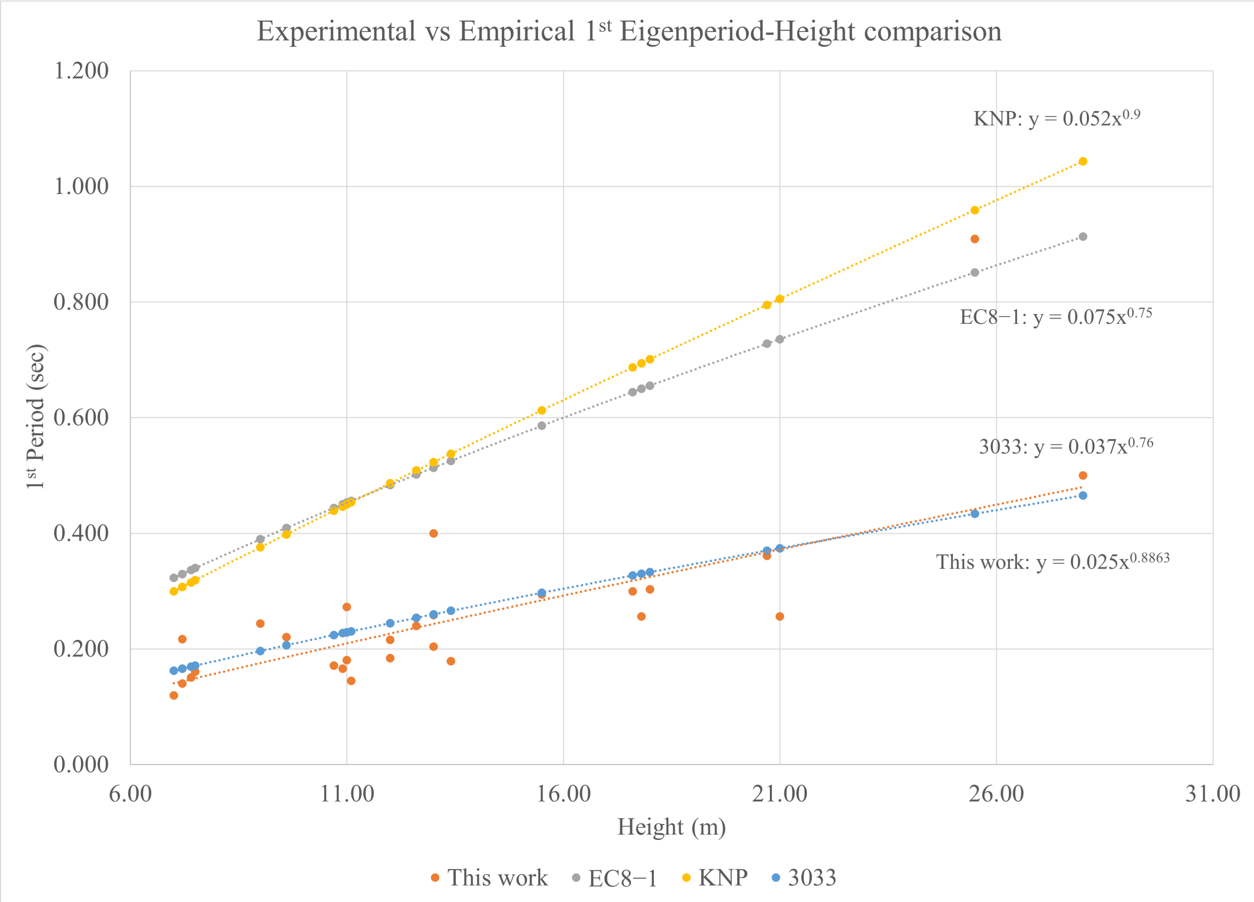


**Figure A1.** Experimental vs Empirical 1st Period-Height comparison.

*Appendix A.2. Sensitivity Analysis*

After noticing the difference between experimental and empirical fundamental periods, in this section the influence of the parameters $C_t$ and $\beta$ over the empirical relationship of eigenperiod prediction is examined. After converting effective stiffness to the geometrical one for the calculation of code-predicted period values, the ratios of experimental periods over predicted ones are calculated. For all these ratios, mean, max and min values are also calculated. In the end, the mean value is set equal to one by means of a "$what - if$" analysis in order to define the values of $C_t$ and $\beta$.

Accordingly, in Table A2, $R_1^{EC8}$ and $R_2^{EC8}$ stand for the $T_{amb}/T_{EC8}(K_{eff})$ and the $T_{amb}/T_{EC8}(K_g)$ ratios, respectively; $C_{t,new}$ is the new value after correction. Mean $R_1^{EC8}$ is 0.49, max value 1.07 and min one 0.32. On the other hand, mean $R_2^{EC8}$ is 0.69, max value 1.51 and min one 0.45. The new value of $C_{t,new}$ is calculated in that way so the mean of $R_2^{EC8}$s is equal to 1.00. After that, $T_{K_g,new}^{EC8}$ and $T_{K_{eff},new}^{EC8}$ are the calculated using the $C_{t,new}^{EC8}$ and $R_{2,new}^{EC8}$ is the updated value of $R_2^{EC8}$ derived using $C_{t,new}^{EC8}$.

**Table A2.** Investigation on the $C_t$ value used for estimating the effective 1st period based on empirical relationship of EC8-1 for the 27 RC buildings.

| No. | $R_1^{EC8}$ | $T_{K_g}^{EC8}$ (s) | $R_2^{EC8}$ | $C_{t,new}^{EC8}$ | $T_{K_g,new}^{EC8}$ (s) | $T_{K_{eff},new}^{EC8}$ (s) | $R_{2,new}^{EC8}$ |
|---|---|---|---|---|---|---|---|
| 1 | 0.349 | 0.520 | 0.493 | 0.037 | 0.361 | 0.510 | 0.711 |
| 2 | 0.395 | 0.460 | 0.558 | 0.042 | 0.319 | 0.451 | 0.805 |
| 3 | 0.462 | 0.463 | 0.654 | 0.049 | 0.321 | 0.454 | 0.943 |
| 4 | 0.548 | 0.646 | 0.775 | 0.058 | 0.448 | 0.633 | 1.117 |
| 5 | 1.068 | 0.602 | 1.511 | 0.113 | 0.417 | 0.590 | 2.179 |
| 6 | 0.472 | 0.240 | 0.668 | 0.050 | 0.167 | 0.236 | 0.963 |
| 7 | 0.369 | 0.318 | 0.521 | 0.039 | 0.221 | 0.312 | 0.752 |
| 8 | 0.387 | 0.314 | 0.547 | 0.041 | 0.218 | 0.308 | 0.789 |
| 9 | 0.448 | 0.238 | 0.634 | 0.048 | 0.165 | 0.233 | 0.914 |
| 10 | 0.503 | 0.363 | 0.712 | 0.053 | 0.252 | 0.356 | 1.026 |
| 11 | 0.626 | 0.276 | 0.885 | 0.066 | 0.191 | 0.270 | 1.277 |
| 12 | 0.496 | 0.515 | 0.701 | 0.053 | 0.357 | 0.505 | 1.012 |
| 13 | 0.425 | 0.233 | 0.602 | 0.045 | 0.162 | 0.229 | 0.868 |
| 14 | 0.340 | 0.371 | 0.481 | 0.036 | 0.258 | 0.364 | 0.693 |
| 15 | 0.397 | 0.363 | 0.562 | 0.042 | 0.252 | 0.356 | 0.811 |
| 16 | 0.539 | 0.289 | 0.763 | 0.057 | 0.201 | 0.284 | 1.100 |
| 17 | 0.370 | 0.228 | 0.523 | 0.039 | 0.158 | 0.224 | 0.755 |
| 18 | 0.465 | 0.456 | 0.657 | 0.049 | 0.316 | 0.447 | 0.948 |
| 19 | 0.601 | 0.320 | 0.851 | 0.064 | 0.222 | 0.314 | 1.227 |
| 20 | 0.446 | 0.342 | 0.631 | 0.047 | 0.237 | 0.335 | 0.910 |
| 21 | 0.399 | 0.320 | 0.564 | 0.042 | 0.222 | 0.314 | 0.814 |
| 22 | 0.381 | 0.342 | 0.538 | 0.040 | 0.237 | 0.335 | 0.776 |
| 23 | 0.502 | 0.414 | 0.710 | 0.053 | 0.287 | 0.406 | 1.024 |
| 24 | 0.318 | 0.323 | 0.449 | 0.034 | 0.224 | 0.316 | 0.648 |
| 25 | 0.478 | 0.355 | 0.677 | 0.051 | 0.246 | 0.348 | 0.976 |
| 26 | 0.778 | 0.363 | 1.100 | 0.083 | 0.252 | 0.356 | 1.587 |
| 27 | 0.658 | 0.233 | 0.931 | 0.070 | 0.162 | 0.229 | 1.342 |

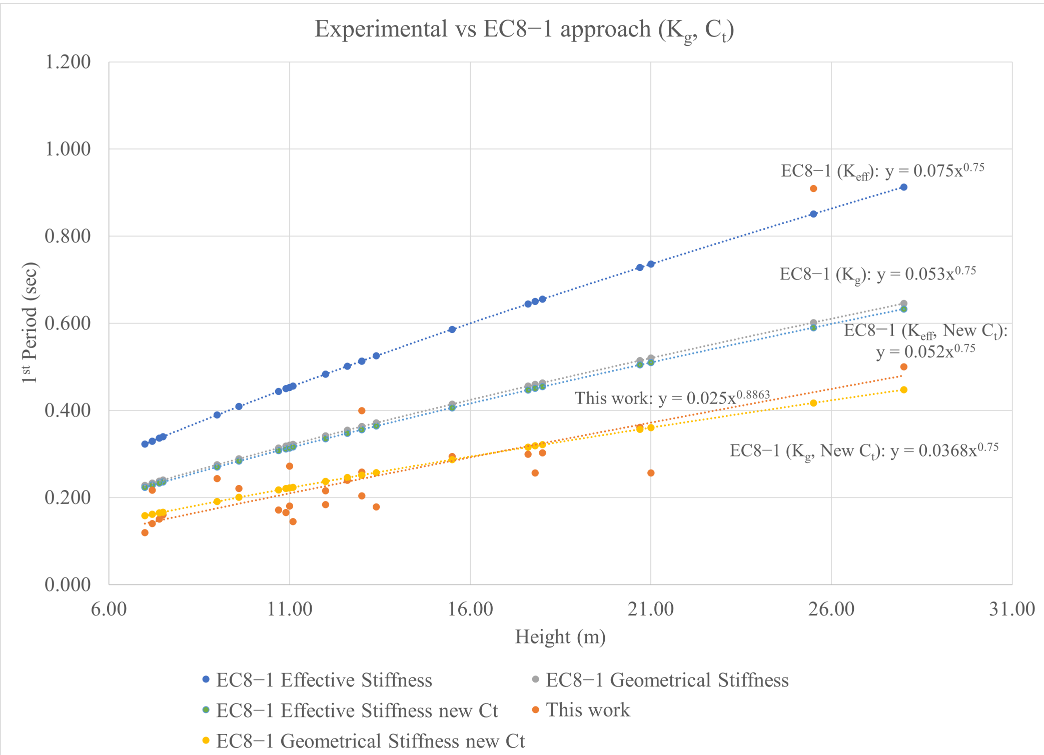


**Figure A2.** Experimental vs EC8's expression ($Kg$, $C_t$).

A very similar to the expression of Equation (3) suggested by EC8, is suggested for the case of KAN.EPE [21] (subsequently labeled as KNP); the following expression is used for estimating the basic eigenperiod:

$$T_1 = C_t \times H^{\beta} \tag{A2}$$

where for RC buildings it is suggested to use the following values, $C_t$ = 0.052 and $\beta$=0.90, while the height $H$ is provided in meters ($m$).

The corresponding investigation can be found in Table A3, $R_1^{KNP}$ stands for the $T_{amb}/T_{KNP}(K_{eff})$ ratio, $R_2^{KNP}$ stands for the $T_{amb}/T_{KNP}(K_g)$ ratio, $C_{t,new}^{KNP}$ is the new value after the correction, $T_{K_g,new}^{KNP}$ and $T_{K_{eff},new}^{KNP}$ are the new values of using the $C_{t,new}^{KNP}$ and $R_{2,new}^{KNP}$ is the updated value of $R_2^{KNP}$ derived using $C_{t,new}^{KNP}$. Given that the empirical expression of KAN.EPE is a function of parameter $\beta$, it is examined the influence of its updated value on the estimation of effective 1st eigenperiod derived; thus, $T_{K_g,\beta,new}^{KNP}$ and $T_{K_{eff},\beta,new}^{KNP}$ denote the updated values and $R_{2,\beta,new}^{KNP}$ is the corresponding value of the ratio. Before the correction, mean $R_1^{KNP}$ was 0.48, max value 0.95 and min value 0.32. For the $R_2^{KNP}$s, the mean value was 0.68, max value was 1.34 and min value was 0.45. After the calculation of the new $C_{t,new}^{KNP}$, the $R_{2,new}^{KNP}$s had a mean value 1.01, a max value of 1.99 and a min value of 0.67. Following that, $\beta$ was calculated in order the mean of $R_{2,new}^{KNP}$s to be equal to 1.00.

**Table A3.** Investigation on the $C_t$ value used for estimating the effective 1st period based on empirical relationship of KAN.EPE for the 27 RC buildings.

| No. | $R_1^{KNP}$ | $T_{K_g}^{KNP}$ (s) | $R_2^{KNP}$ | $C_{t,new}^{KNP}$ | $T_{K_g,new}^{KNP}$ (s) | $T_{K_{eff},new}^{KNP}$ (s) | $R_{2,new}^{KNP}$ | $T_{K_g,\beta,new}^{KNP}$ (s) | $T_{K_{eff},\beta,new}^{KNP}$ (s) | $R_{2,\beta,new}^{KNP}$ |
|---|---|---|---|---|---|---|---|---|---|---|
| 1 | 0.318 | 0.569 | 0.450 | 0.023 | 0.383 | 0.542 | 0.669 | 0.389 | 0.559 | 0.658 |
| 2 | 0.369 | 0.491 | 0.522 | 0.027 | 0.330 | 0.467 | 0.776 | 0.335 | 0.481 | 0.765 |
| 3 | 0.432 | 0.496 | 0.611 | 0.032 | 0.334 | 0.472 | 0.908 | 0.339 | 0.486 | 0.895 |
| 4 | 0.479 | 0.738 | 0.678 | 0.035 | 0.497 | 0.702 | 1.007 | 0.505 | 0.726 | 0.990 |
| 5 | 0.948 | 0.678 | 1.340 | 0.070 | 0.456 | 0.646 | 1.991 | 0.464 | 0.667 | 1.958 |
| 6 | 0.503 | 0.225 | 0.712 | 0.037 | 0.152 | 0.215 | 1.058 | 0.153 | 0.219 | 1.047 |
| 7 | 0.372 | 0.316 | 0.525 | 0.027 | 0.212 | 0.300 | 0.781 | 0.215 | 0.308 | 0.771 |
| 8 | 0.391 | 0.310 | 0.553 | 0.029 | 0.209 | 0.295 | 0.821 | 0.212 | 0.303 | 0.811 |
| 9 | 0.479 | 0.223 | 0.677 | 0.035 | 0.150 | 0.212 | 1.006 | 0.151 | 0.216 | 0.996 |
| 10 | 0.494 | 0.370 | 0.699 | 0.036 | 0.249 | 0.352 | 1.038 | 0.252 | 0.361 | 1.024 |
| 11 | 0.649 | 0.266 | 0.918 | 0.048 | 0.179 | 0.253 | 1.364 | 0.181 | 0.258 | 1.349 |
| 12 | 0.454 | 0.562 | 0.642 | 0.033 | 0.378 | 0.535 | 0.954 | 0.384 | 0.552 | 0.939 |
| 13 | 0.456 | 0.217 | 0.645 | 0.034 | 0.146 | 0.207 | 0.959 | 0.148 | 0.211 | 0.949 |
| 14 | 0.332 | 0.380 | 0.470 | 0.024 | 0.256 | 0.362 | 0.698 | 0.259 | 0.371 | 0.689 |
| 15 | 0.390 | 0.370 | 0.552 | 0.029 | 0.249 | 0.352 | 0.820 | 0.252 | 0.361 | 0.809 |
| 16 | 0.554 | 0.282 | 0.784 | 0.041 | 0.189 | 0.268 | 1.164 | 0.192 | 0.274 | 1.151 |
| 17 | 0.399 | 0.212 | 0.564 | 0.029 | 0.143 | 0.202 | 0.838 | 0.144 | 0.206 | 0.829 |
| 18 | 0.436 | 0.486 | 0.616 | 0.032 | 0.327 | 0.462 | 0.916 | 0.332 | 0.476 | 0.902 |
| 19 | 0.605 | 0.318 | 0.856 | 0.045 | 0.214 | 0.303 | 1.272 | 0.217 | 0.310 | 1.256 |
| 20 | 0.443 | 0.344 | 0.627 | 0.033 | 0.232 | 0.328 | 0.932 | 0.235 | 0.336 | 0.920 |
| 21 | 0.402 | 0.318 | 0.568 | 0.030 | 0.214 | 0.303 | 0.844 | 0.217 | 0.310 | 0.833 |
| 22 | 0.378 | 0.344 | 0.535 | 0.028 | 0.232 | 0.328 | 0.795 | 0.235 | 0.336 | 0.784 |
| 23 | 0.480 | 0.433 | 0.679 | 0.035 | 0.292 | 0.412 | 1.008 | 0.296 | 0.424 | 0.994 |
| 24 | 0.319 | 0.321 | 0.452 | 0.023 | 0.216 | 0.305 | 0.671 | 0.219 | 0.313 | 0.663 |
| 25 | 0.472 | 0.360 | 0.667 | 0.035 | 0.242 | 0.342 | 0.991 | 0.245 | 0.351 | 0.978 |
| 26 | 0.764 | 0.370 | 1.080 | 0.056 | 0.249 | 0.352 | 1.605 | 0.252 | 0.361 | 1.584 |
| 27 | 0.706 | 0.217 | 0.998 | 0.052 | 0.146 | 0.207 | 1.483 | 0.148 | 0.211 | 1.468 |

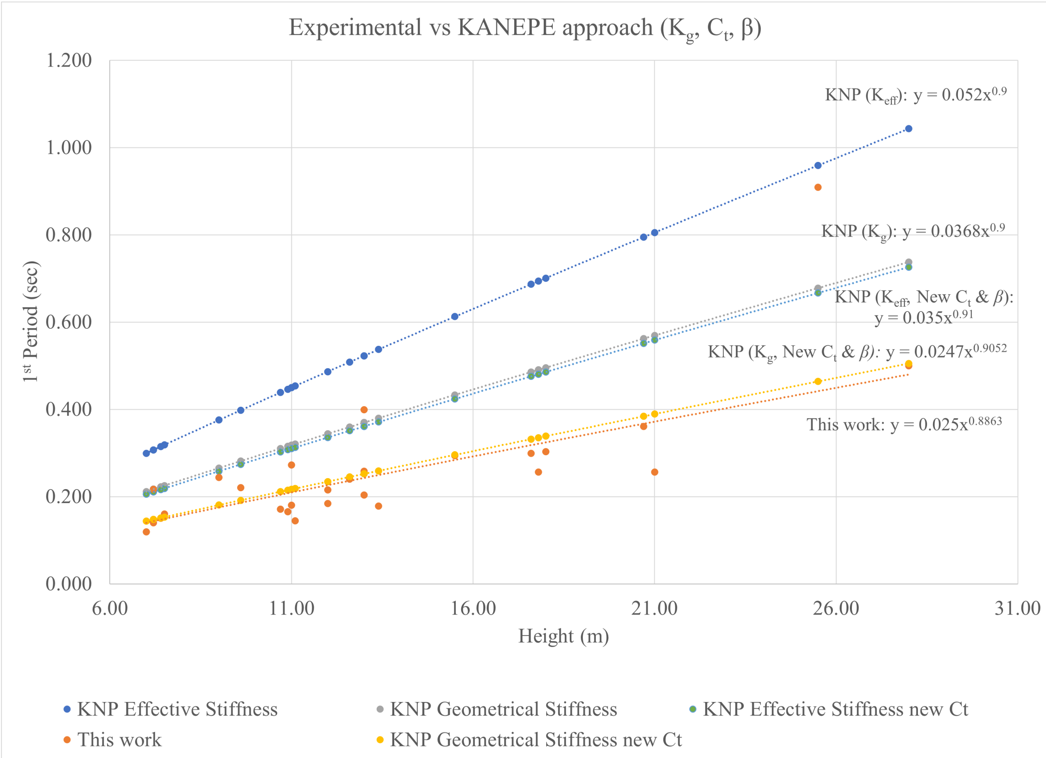


**Figure A3.** Experimental vs KAN.EPE's expression ($Kg$, $C_t$, $\beta$).

## References


1. Rasulo, A.; Testa, C.; Borzi, B. Seismic Risk Analysis at Urban Scale in Italy. In *Proceedings of the Computational Science and Its Applications—ICCSA 2015, Banff, AB, Canada, 22–25 June 2015*; Gervasi, O., Murgante, B., Misra, S., Gavrilova, M.L., Rocha, A.M.A.C., Torre, C., Taniar, D., Apduhan, B.O., Eds.; Springer International Publishing: Cham, Switzerland, 2015; pp. 403–414.
2. Rasulo, A.; Fortuna, M.A.; Borzi, B. A Seismic Risk Model for Italy. In *Proceedings of the Computational Science and Its Applications—ICCSA, Beijing, China, 4–7 July 2016*; Gervasi, O., Murgante, B., Misra, S., Rocha, A.M.A., Torre, C.M., Taniar, D., Apduhan, B.O., Stankova, E., Wang, S., Eds.; Springer International Publishing: Cham, Switzerland, 2016; pp. 198–213.
3. United States Geological Survey. Earthquake Counts by U.S. State. 2019. Available online: https://www.usgs.gov/natural-hazards/earthquake-hazards/lists-maps-and-statistics (accessed on 1 March 2022).
4. FEMA. *B-526, Earthquake Safety Checklist*; Department of Homeland Security, Federal Emergency Management Agency, Mitigation Division: Washington, DC, USA, 2017.
5. Department of Homeland Security USA. Ready Campaign. 2020. Available online: https://www.ready.gov/earthquakes (accessed on 1 March 2022).
6. Allaf, N.; Charleson, A. Seismic retrofitting and the integration of architecture and structure. In Proceedings of the Conference of the New Zealand Society for Earthquakel Engineering, Christchurch, New Zealand, 1–3 April 2016.
7. Erdik, M. Earthquake risk assessment. *Bull. Earthq. Eng.* **2017**, *15*, 5055–5092. [CrossRef]
8. Lagaros, N.D.; Charmpis, D.C.; Chatzieleftheriou, S.; Damikoukas, S. Vulnerability assessment of structures with stochastic properties subjected to random seismic excitation. *Procedia Manuf.* **2020**, *44*, 671–678. [CrossRef]
9. FEMA. *P-154: Rapid Visual Screening of Buildings for Potential Seismic Hazards: A Handbook*; Federal Emergency Management Agency: Washington, DC, USA, 2015.
10. Knott, C. Seismic Hazard Assessment of Oregon: Analysis of Earthquake Resilience within State Wide Infrastructure and the Cost of Retrofitting. *Acad. Excell. Showc. Proc.* **2020**, *258*. Available online: https://digitalcommons.wou.edu/aes/258 (accessed on 1 March 2022).
11. Greek Earthquake Planning and Protection Organization (EPPO). *Pre-Seismic Inspection of Public and Beneficial Buildings*; Greek Earthquake Planning and Protection Organization (EPPO): Athens, Greece, 2022.
12. Demartinos, K.; Dritsos, S. First-Level Pre-earthquake Assessment of Buildings Using Fuzzy Logic. *Earthq. Spec.* **2006**, *22*, 865–885. [CrossRef]
13. Standoli, G.; Giordano, E.; Milani, G.; Clementi, F. Model Updating of Historical Belfries Based on OMA Identification Techniques. *Int. J. Archit. Herit.* **2020**, *15*, 1–25. [CrossRef]
14. Lenci, S.; Consolini, L.; Clementi, F. On the experimental determination of dynamical properties of laminated glass. *Ann. Solid Struct. Mech.* **2015**, *7*, 27–43. [CrossRef]

15. Marcheggiani, L.; Clementi, F.; Formisano, A. Static and dynamic testing of highway bridges: A best practice example. *J. Civ. Struct. Health Monit.* **2020**, *10*, 43–56.
16. Gentile, C.; Saisi, A. Ambient vibration testing of historic masonry towers for structural identification and damage assessment. *Constr. Build. Mater.* **2007**, *21*, 1311–1321. [CrossRef]
17. Beskhyroun, S.; Navabian, N.; Wotherspoon, L.; Ma, Q. Dynamic behaviour of a 13-story reinforced concrete building under ambient vibration, forced vibration, and earthquake excitation. *J. Build. Eng.* **2020**, *28*, 101066. [CrossRef]
18. Ferraioli, M.; Miccoli, L.; Abruzzese, D.; Mandara, A. Dynamic characterisation and seismic assessment of medieval masonry towers. *Nat. Hazards* **2017**, *86*, 489–515. [CrossRef]
19. Gentile, C.; Saisi, A.; Cabboi, A. Structural identification of a masonry tower based on operational modal analysis. *Int. J. Archit. Herit.* **2015**, *9*, 98–110. [CrossRef]
20. FEMA 356. *Prestandard and Commentary for the Seismic Rehabilitation of Buildings*; Federal Emergency Management Agency: Washington, DC, USA, 2000.
21. EPPO. *Code for Structural Interventions (KAN.EPE)*; Earthquake Protection and Planning Organization: Athens, Greece, 2017.
22. Chatzieleftheriou, S.; Damikoukas, S. Optimal Sensor Installation to Extract the Mode Shapes of a Building–Rotational DOFs, Torsional Modes and Spurious Modes Detection. Technical report, Unquake (Structures & Sensors P.C.). 2021. Available online: https://www.researchgate.net/institution/Unquake/post/6130bc2ca1abfe50c1559a26_Download_White_Paper_Optimal_sensor_installation_to_extract_the_mode_shapes_of_a_building-Rotational_DOFs_torsional_modes_and_spurious_modes_detection (accessed on 1 March 2022).
23. FEMA. *Hazus—MH 2.1: Technical Manual*; Department of Homeland Security, Federal Emergency Management Agency, Mitigation Division: Washington, DC, USA, 2013.
24. Esteghamati, M.Z.; Lee, J.; Musetich, M.; Flint, M.M. INSSEPT: An open-source relational database of seismic performance estimation to aid with early design of buildings. *Earthq. Spec.* **2020**, *36*, 2177–2197. [CrossRef]
25. Omoya, M.; Ero, I.; Esteghamati, M.Z.; Burton, H.V.; Brandenberg, S.; Sun, H.; Yi, Z.; Kang, H.; Nweke, C.C. A relational database to support post-earthquake building damage and recovery assessment. *Earthq. Spec.* **2022**, *38*, 1549–1569. [CrossRef]
26. Unquake. Unquake Accelerograph-Accelerometer Specifications. Available online: https://www.unquake.co (accessed on 1 March 2022).
27. Whittaker, E.T. XVIII.—On the Functions which are represented by the Expansions of the Interpolation-Theory. *Proc. R. Soc. Edinb.* **1915**, *35*, 181–194. [CrossRef]
28. Blu Tack. Blu Tack®. 2020. Available online: http://www.blu-tack.co.uk/ (accessed on 1 March 2022).
29. Bulajić, B.D.; Todorovska, M.I.; Manić, M.I.; Trifunac, M.D. Structural health monitoring study of the ZOIL building using earthquake records. *Soil Dyn. Earthq. Eng.* **2020**, *133*, 106105. [CrossRef]
30. Trifunac, M.D.; Todorovska, M.I.; Manić, M.I.; Bulajić, B.D. Variability of the fixed-base and soil–structure system frequencies of a building—The case of Borik-2 building. *Struct. Control. Health Monit.* **2010**, *17*, 120–151. [CrossRef]
31. ATC-40. *Seismic Evaluation and Retrofit of Concrete Buildings*; Applied Technology Council (ATC): Redwood City, CA, USA, 1996.
32. Fajfar, P.; Gašperšič, P. The N2 method for the seismic damage analysis of RC buildings. *Earthq. Eng. Struct. Dyn.* **1996**, *25*, 31–46. [CrossRef]
33. Kreslin, M.; Fajfar, P. The extended N2 method considering higher mode effects in both plan and elevation. *Bull. Earthq. Eng.* **2012**, *10*, 695–715. [CrossRef]
34. European Committee for Standardization (CEN). *Eurocode 8: Design of Structures for Earthquake Resistance, Part 1: General Rules, Seismic Actions and Rules for Buildings)*; European Committee for Standardization (CEN): Brussels, Belgium, 2004.
35. Uniform Building Code. *Uniform Building Code (UBC-97)*; Whitter: Whitter, CA, USA, 1997.
36. National Research Council of Canada (NRC/IRC). *National Building Code of Canada*; National Research Council of Canada (NRC/IRC): Ontario, OT, Canada, 2005.
37. Chiauzzi, L.; Masi, A.; Mucciarelli, M.; Cassidy, J.; Kutyn, K.; Traber, J.; Ventura, C.; Yao, F. Estimate of Fundamental Period of Reinforced Concrete Buildings: Code Provisions vs. Experimental Measures in Victoria and Vancouver (BC, Canada). In Proceedings of the 15th World Conference on Earthquake Engineering, Lisbon, Portugal, 24–28 September 2012.